

Detection of tube defect using the autoregressive algorithm

Zakiah A. Halim ^{*1}, Nordin Jamaludin ^{2a}, Syarif Junaidi ^{2b} and Syed Yusainee ^{3c}

¹ Faculty of Mechanical Engineering, Universiti Teknikal Malaysia Melaka,
Hang Tuah Jaya, 76100 Durian Tunggal, Melaka, Malaysia

² Department of Mechanical Engineering & Materials, Faculty of Engineering and Built,
Universiti Kebangsaan Malaysia, 43000 UKM, Bangi, Selangor, Malaysia

² Faculty of Applied Science, Universiti Teknologi MARA, 42300 Shah Alam, Selangor, Malaysia

(Received March 27, 2014, Revised October 21, 2014, Accepted December 29, 2014)

Abstract. Easy detection and evaluation of defect in the tube structure is a continuous problem and remains a significant demand in tube inspection technologies. This study is aimed to automate defect detection using the pattern recognition approach based on the classification of high frequency stress wave signals. The stress wave signals from vibrational impact excitation on several tube conditions were captured to identify the defect in ASTM A179 seamless steel tubes. The variation in stress wave propagation was captured by a high frequency sensor. Stress wave signals from four tubes with artificial defects of different depths and one reference tube were classified using the autoregressive (AR) algorithm. The results were demonstrated using a dendrogram. The preliminary research revealed the natural arrangement of stress wave signals were grouped into two clusters. The stress wave signals from the healthy tube were grouped together in one cluster and the signals from the defective tubes were classified in another cluster. This approach was effective in separating different stress wave signals and allowed quicker and easier defect identification and interpretation in steel tubes.

Keywords: autoregressive; defect identification; impact excitation; pattern recognition; stress wave

1. Introduction

Tubes are the most efficient method of transferring fluids between equipment such as heat exchangers and boilers in many processing industries. Both the inner and outer sides of the tubes are exposed to fluid, which could be the process chemicals, water, steam or air in either side of the tubes. Hence, these tubes are vulnerable to service-induced discontinuities such as pitting, corrosion and crack. These types of discontinuities are major concerns in the industries as they affect tube integrity. The presence of pitting, corrosion and crack do not only cause disruption of operation, property damage and associated containment and revenue loss, but more importantly safety hazards and loss of life.

*Corresponding author, Ph.D. Student, E-mail: zakiah@utem.edu.my

^a Ph.D., E-mail: nordin@eng.ukm.my

^b Ph.D., E-mail: syarif@eng.ukm.my

^c Ph.D., E-mail: syedy237@salam.uitm.edu.my

In order to protect tube integrity, maintenance must be done periodically. Generally, tube inspection is the conventional method to inspect and assure the tubes are safe to operate (Bulloch *et al.* 2009, Cicero *et al.* 2010, Allahkaram *et al.* 2011). Tube inspection is the activity of gathering information about the condition of the tubes. Adequate inspection instruments and measuring apparatus are used in order to assess the health and functioning state of the tube structure. The outcomes from tube inspection will assist future maintenance decisions on tube integrity. The maintenance of tubes is expected to sustain tube health and subsequently its life, with fewer failures at lower costs.

Liquid penetrant testing (LPT) and magnetic particles inspection (MPI) are usually carried out for external tube surface examination. The testing were done at external location such as tube support parts and components (Antaki 2005). In addition, ultrasonic testing (UT) is also carried out at selected accessible external tube locations (Xueqin *et al.* 2008). For internal tube integrity assessment, various tube inspection methods such as internal rotating inspection system (IRIS), magnetic flux leakage (MFL), eddy current (EC) and remote field electromagnetic testing (RFET) have been generally accepted as the standards worldwide. The successful application of these methods requires a good understanding of the underlying physical process. IRIS method is based on ultrasonic wave propagation (Birring 1999) whereas MFL, ECT and RFET methods are based on electromagnetic waves principle (Zhang *et al.* 2007, Wilson and Tian 2007, Gotoh and Takahashi 2007, Yang and Li 2013). These methods require insertion of the inspection probe into each of the tubes and are pulled back across the length. The signal is captured as the probe moves in traversal across the tube length. Necessary training is required before a personnel is qualified to administer and infer the condition of the tubes using the methods (Carino 2013). Moreover, the tube surface needs to be cleaned until the bare metal prior to the testing. The surface preparation is prone to increase the wall thinning problem.

Typical defect evaluation depends on the response signals due to interactions of the abnormalities with physical processes as described by Zhang *et al.* (2007). The studies focused on the physical features extracted from the response signals such as time of arrival (TOA). The problem with this approach is that signal interpretation is done manually and relies heavily on the proficiencies of the personnel to identify the exact TOA. The actual TOA may be distorted due to traversal probe pulling speed as well as internal debris and corrosive elements. Inconsistent and unsuitable traversal pulling speed interferes with the exact TOA and misleads signal interpretation. Additionally, debris and corrosive elements could also mask the defect signal during the traversal movement. Hence, interpretation and evaluation of captured signals are very subjective and personnel-dependent. Despite the necessary training, the skills and experiences of the personnel also affects the interpretation and evaluation of the inspected tubes.

The employment of B-scan and C-scan displays in the IRIS method as described by Birchall (2007) enable personnel to visualise cross section and topography of the tubes. The display in B-scan provides surface reflection within the tube in the scanned line. The variation of reflection's amplitude exposes a detailed cross section of the tube over a single axis. Besides, C-scan is another presentation alternative that displays the top view of the tested tube. In the C-scans, the transducer is swept across in the x -direction and stepped in the y -direction after each sweep. The generated image represents the signal amplitude or depth at each point of the test position. In both displays, colours are used to represent the signal amplitude of the measured depth.

However, the slow pulling speed and extensive cleaning prior to inspection have limited the usage of this method. The method is time-consuming and excessive tube re-cleaning would inappropriately remove the remaining thickness of the tubes. Recent studies by Gotoh and

Takahashi (2007) and Ryu *et al.* (2009) proposed the finite element method by simulating the electromagnetic field from the outer side of the tubes. Leakage in the electromagnetic field makes it possible for defect identification. However, the existence of a support plate in the heat exchanger affects the electromagnetic field, which makes the technique impractical in actual heat exchangers.

Therefore, a more practical identification and evaluation technique is the main challenge in tube inspection services. Easy, quick and correct interpretation as well as evaluation of tube inspection findings are essential in tube integrity assessment. Several different procedures and signal processing approaches have shown considerable success in identifying the defect in tube and pipeline system, for instance using shifting in frequency spectrum, cross-correlation and short-time Fourier transform (Gao *et al.* 2005, Mahjoob *et al.* 2007, Lee *et al.* 2008, Shehadeh *et al.* 2008, Da Silva *et al.* 2009). It appears from the aforementioned investigations that most attention has been paid to frequency domain analysis at low-frequency stress wave to provide condition information of a hollow-like system. However, very limited work was conducted on pattern recognition to characterise defect signals using high-frequency stress waves (Da Silva *et al.* 2006).

Accordingly, the present paper proposes a pattern recognition technique to automate defect identification using the autoregressive (AR) algorithm. To demonstrate this, a newly developed method namely Vibration Impact Acoustic Emission (VIAE) is introduced. VIAE is developed to acquire acoustic emission signals from impact excitation. The primary concern in this method is the characteristics of high frequency stress wave activity instead of low frequency stress wave activity that is already well-established for tube-like structures. VIAE testing has been conducted on a series of ASTM A179 seamless steel tubes. Specifically, four tubes with artificial defects of different depths and one healthy reference tube were used throughout the experiment. Vibrational impact is introduced to excite stress wave propagation in the tube structure. The resultant stress waves were captured by a high frequency sensor and were classified using the AR algorithm. The classification process was employed to evaluate whether the AR coefficient associated with stress wave signals was adequately robust to group defects with known depth into the appropriate natural clusters. The study of high frequency stress wave propagation in small diameter tubes is the first of its kind and authors are unaware of any published reports pertaining to the analysis using the acoustic emission signals and using AR method as a defect identification tool. The classification results were presented graphically using a dendrogram that disclosed the natural clusters of the stress wave signals. This approach demonstrates the effective discrimination of stress wave propagation path into recognized pattern that allows for quicker, more confident and easier defect identification in steel tubes.

2. Autoregressive model

The AR model approach is the most promising alternative as an automated defect identification tool due to its simplicity in formulation. The AR model represents a stationary discrete-time stochastic process with certain corresponding forward prediction error (FPE). A stationary random process $x(n)$ may be described as an AR model of order M if its sample $x(n)$ at time n is regressed on M past samples, $x(n-1)$, $x(n-2)$, ..., $x(n-M)$. This is expressed as

$$x(n) = \sum_{k=1}^M h(k)x(n-k) + W(n) \quad (1)$$

in which $W(n)$ is a white noise process of zero mean and variance σ^2 and serves as the input, $h(k)$ are the AR coefficients and M is the model order.

The model order M is always unknown and has to be estimated using the FPE. The FPE is selection criteria method based on residual variance in the expected prediction error (Broersen 2006). The shape of a signal can be correctly represented by AR coefficients as long as the model order M is sufficiently large. Hence, it is important to determine the correct model order to represent the stress wave signals. The Levinson-Durbin algorithm provides the most efficient solution for Eq. (1) to represent the shape of the stress wave signals by a set of AR coefficients. The AR coefficients are computed recursively by setting M to zero. The incremental process is continued until the residual variance does not change over the repeated process, thus indicating the correct model order.

Previous studies have primarily concentrated on AR modelling as condition monitoring of rotating machinery (Jamaludin and Mba 2002a, b, Thanagasundram and Schindwein 2006a, Zhan and Mechefske 2007, Elforjani and Mba 2010). The sources of stress wave were originated from the interaction of two surfaces that emitted stress wave activities. The AR algorithm is employed due to ability of the AR coefficients to identify and classify stress wave signals generated by different faults condition based on their signatures shape. Jamaludin and Mba (2002a, b) have noted that AR modeling has successfully represented high frequency stress wave signal on low speed roller bearings and provided an identification tool to diagnose bearing deficiencies without prior knowledge of the structural characteristic. Each fault has a distinct signature pattern to successfully differentiate the bearing condition.

Moreover, studies by Thanagasundram and Schindwein (2006a, b) indicated that AR modeling accurately identifies faults at different speed and load of dry vacuum pumps. The stress wave signals are comprised of harmonic sinusoids. The differences in the sharp peaks during the vibration rotational process alters the shape of signals have been appropriately discriminated to indicate the good and faulty bearing conditions. Even though selection of model order is the most critical step in the investigations, the studies found that AR modeling requires much shorter lengths of recorded data than traditional diagnostic tools such as Fast Fourier Transform (FFT) and artificial neural networks, which require large amounts of data training for successful fault prediction. Further work by Zhan and Mechefske (2007) obtained consistent results when similar AR approach was performed for monitoring deterioration in gear boxes. In a more recent work, Elforjani and Mba (2010) have effectively applied the AR modelling approach to locate the source and size of natural faults in low speed bearing whilst in operation.

Moreover, the AR model has been successfully applied as part of structural health monitoring systems of masonry and beam structures (Chen *et al.* 2005, Atamturktur *et al.* 2011). The AR model was applied by Chen *et al.* (2005) to extract natural frequencies to investigate the health condition of beam structures. The authors measured the vibration response of the beams under impact excitation. It is observed that crack parameters in beam structures have been successfully identified by using the changes in the natural frequencies. Atamturktur *et al.* (2011) also investigated the vibration response from vaulted masonry. The authors have employed the AR model to predict signals of undamaged and damaged vaults in order to indicate the structural health state of the vaulted masonry. The observation is in agreement in other studies, which demonstrated that the AR model is capable of accurately detecting the vault condition. The successful application of the AR model in discriminating health and damaged conditions of structures is widely reported in the open literature. However, to the best of the authors' knowledge, the application of AR in tube inspection has not been explored yet and has motivated this study.

3. Materials and methodology

Seamless cold-drawn steel ASTM A179 tubes, which are a typical heat exchanger material used in power plant industries, were used throughout the experiments. The steel tubes are 1 m in length, have a 19.05 mm outer diameter and 2.11 mm tube thickness. One reference tube in good condition is used as a calibration step. The reference tube was used to determine the original stress wave in the healthy tube. Four test tubes containing artificial defect were prepared. An artificial defect was introduced to each test tube by milling a hole to replicate pitting defect as illustrated in Fig. 1. Specifically, Tube 1, Tube 2, Tube 3 and Tube 4 each has an artificial defect located at 100 mm from one of tube ends with varying depth of 20%, 40%, 60% and 100% of the tube thickness, respectively. The cross section views for the defective tubes are demonstrated in Fig. 2. Information on the defect is tabulated in Table 1.

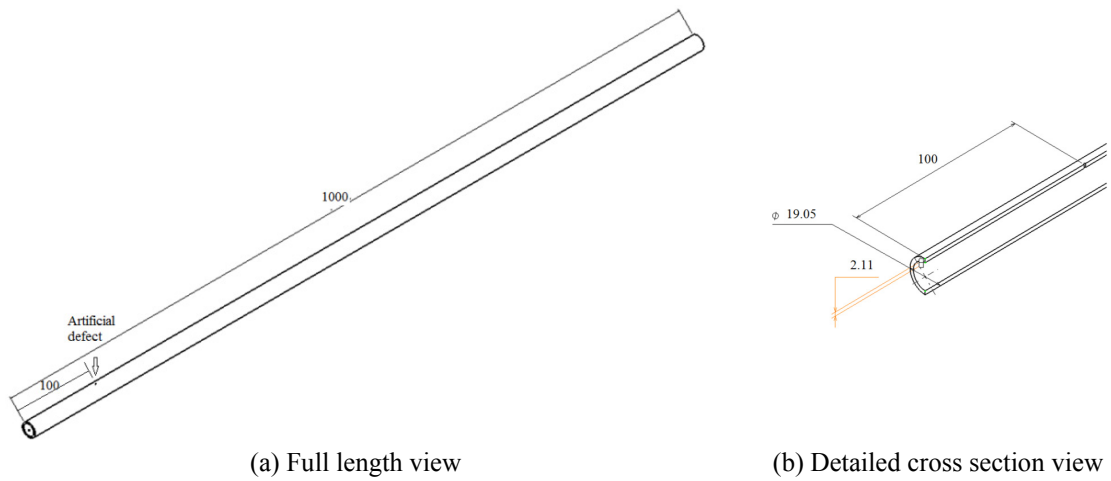


Fig. 1 Transverse view of defective tubes

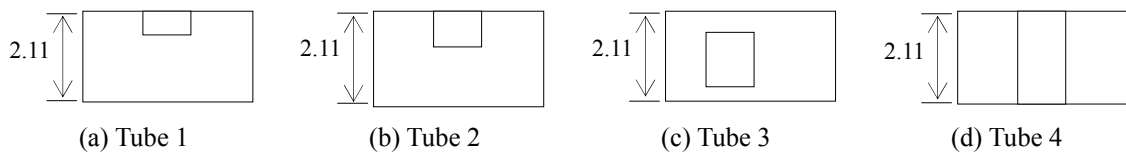


Fig. 2 Cross section view of artificial defects

Table 1 Depth of defect

Tube	Label	Depth (%)	Depth (mm)
Reference tube	R	0	0
Tube 1	A	20	0.42
Tube 2	B	40	0.84
Tube 3	C	60	1.26
Tube 4	D	100	2.11

3.1 Experimental procedure

The Vibration Impact Stress Emission (VIAE) technique was used in this study. The schematic experimental set-up for this study is presented in Fig. 3. Both tube ends were fixed and supported using table vice. The tube was impacted axially by the impact hammer (2 kN, BK 8206-002) at 20 mm from one of the tube ends. The transient stress wave generated from the impact excitation was captured using the acoustic emission (AE) technology system. A small aperture AE sensor (model SE1000-H, frequency range 8-400 kHz) with pre-amplifier (AEP4, gain 34 dB) was fixed at 15 mm from the other tube ends. The AE sensor was placed at the end of tube length to capture the propagating stress wave along the tube structure. The pre-amplifier was used to increase signal voltage and at the same time maintain signal-to-noise ratio. A sampling frequency of 10 MHz was used in this study. The sampling frequency is the maximum setting in the Vallen AMSY-5 multi-channel system. A higher sample rate was chosen as it allows better reconstruction of the captured signals. The AE sensor was connected to the Vallen AMSY-5 multi-channel system, and then connected to a host laptop for post-processing data in the VisualAE software.

Before commencing each test, the filter setting, background noise level and the sensor mounting were controlled. The frequency band measurement in the Vallen AMSY-5 multi-channel system is 18-2400 kHz. A Butterworth band-pass filter (8th order, 48 dB/octave) was used to eliminate unwanted frequency ranges. The frequency configuration for stress wave measurement was set to 18-300 kHz. The embedded digital filter is suitable for capturing low frequency and

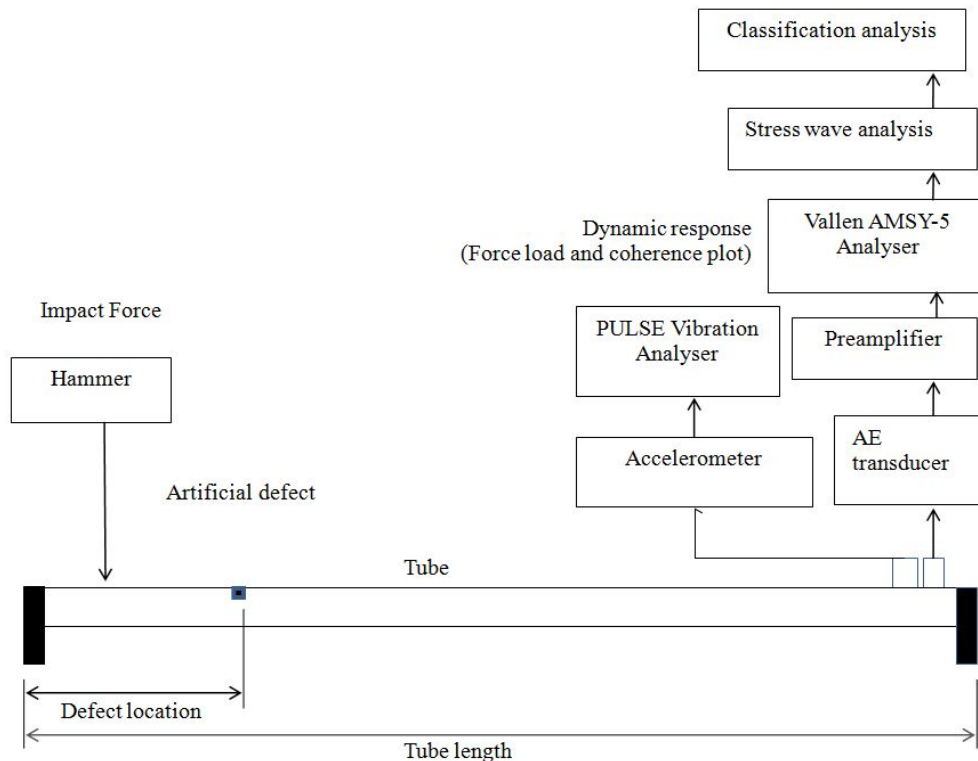


Fig. 3 Experimental set-up

low attenuation stress wave signals from the impact excitation. In addition, the measured background noise level was 24 dB. To prevent background noise crossing signal during measurement, a 6 dB difference is added to the fixed threshold. Hence a fixed 30 dB threshold level is selected for the stress wave measurement. Only signals that have crossed the threshold level will be recorded.

The verification of the AE sensor mounting was done by a Hsu-Nielson source. The pencil lead break test was conducted each time the AE sensor is attached to a different test tube. The lead was extended at 3 mm and maintained at 30° from the test tube surface. The lead break test was repeated for at least 3 times. The lead extension length must be consistent to ensure similar sensor response. Shorter lead extension produces higher amplitude response. The responses to the Hsu-Nielson source are found larger than 97 dB, indicating a good hold-down force contact between the AE sensor and test tubes.

The dynamic response due to the impact was measured by a piezoelectric accelerometer (model BK4508B, frequency range 0-8 kHz) mounted adjacent to the AE sensor at the other tube ends. The accelerometer and impact hammer were connected to an analog-to-digital converter front-end BK Type 3560. The front-end was connected to a different host laptop for data analysis using PULSE Labshop software. The test-rig lay-out is shown in Fig. 4.

The data collected from the PULSE Labshop were input force load and coherency plot. A typical force load for applied impact on the tubes is shown in Fig. 5. Specifically, Figs. 5(a)-(e) clearly showed that the typical time history of the applied impact force load for all the tubes has a time delay of 18 ms and features an average sharp peak of 37 N. The impact was repeated for 20 times for each tube condition. The consistency of the repeated impact that affects the propagation of transient stress wave in the tubes was validated using coherency plot. The coherence plot represents the linear relationship between the impact force load and dynamic response of the signals. The coherence plots in Figs. 6(a)-(e) verified that a uniform impact force load has been applied to the tubes. A value near 1 indicated that the tubes were excited by good quality and consistent impact force loads.

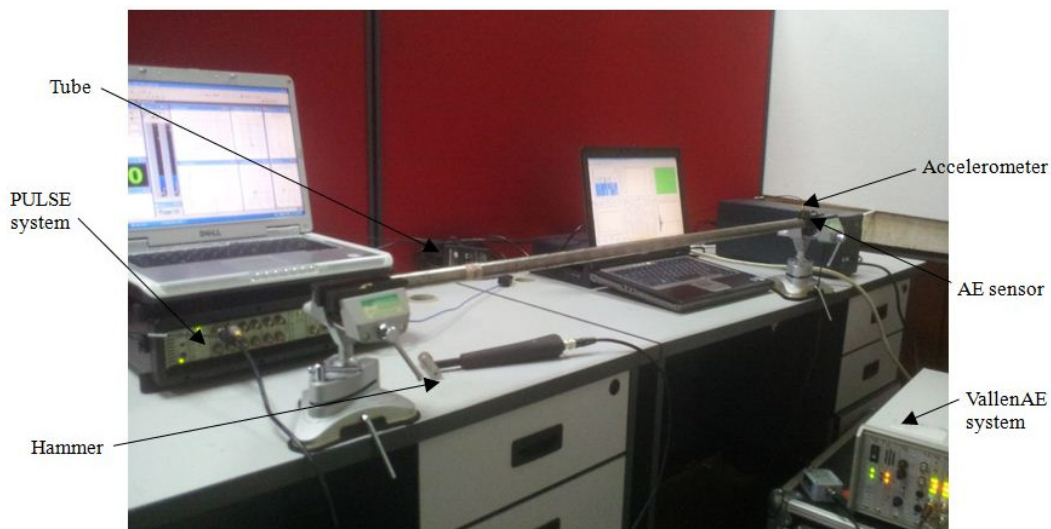


Fig. 4 Test rig lay-out

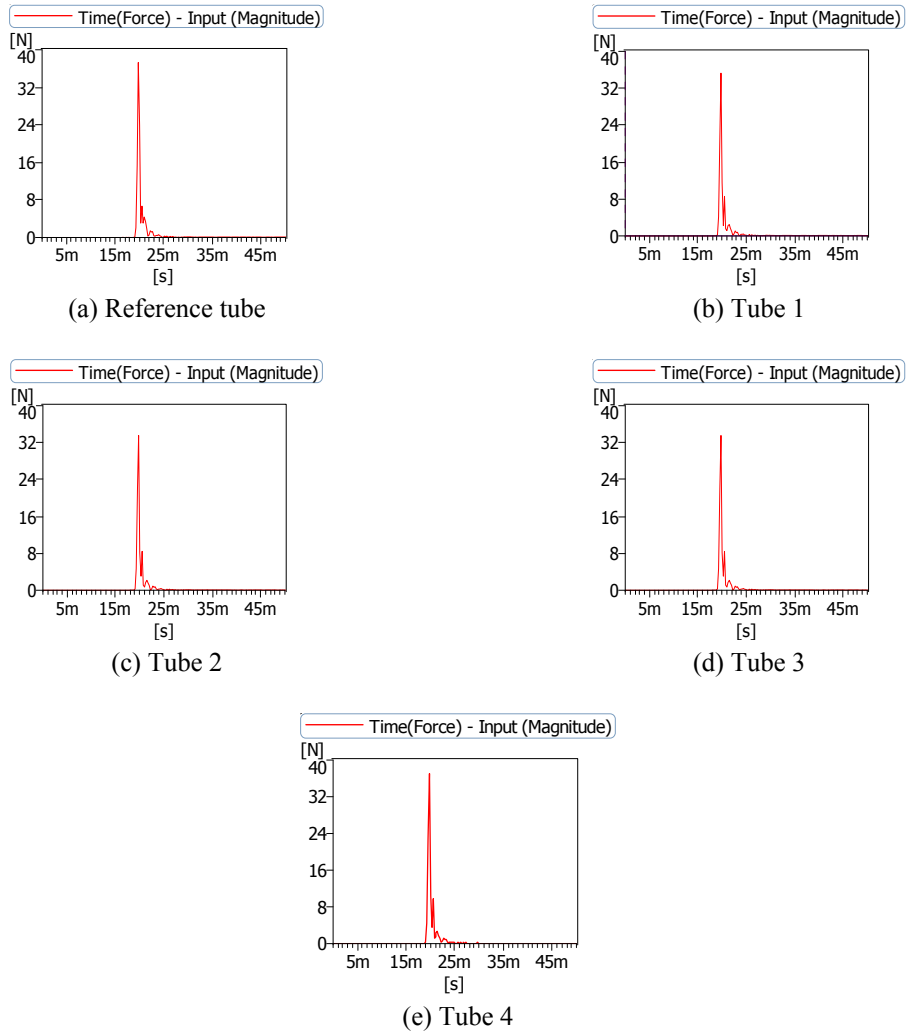


Fig. 5 Time history of impact force loads

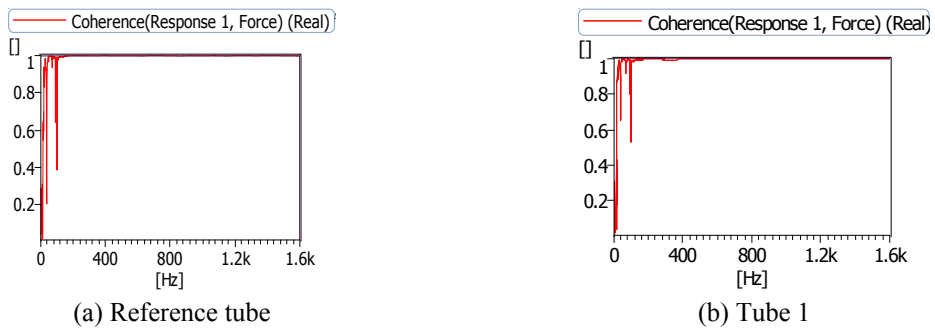


Fig. 6 Consistency of impact force loads

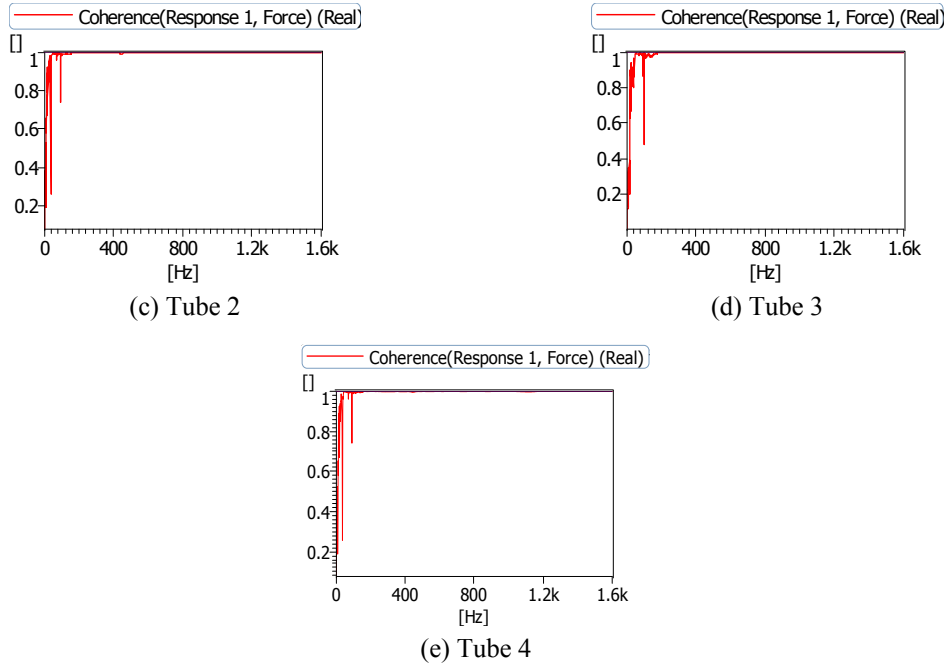


Fig. 6 Continued

In the VisualAE software, the acquired stress wave signal has the sample length of 524,288 μs for every impact. The impact was repeated 20 times for every tube. Hence, each tube has 20 time history of stress wave signals associated with its condition. Each stress wave signal for the reference tube was labelled as R1 to R20. The stress wave signals from the defective Tube 1, Tube 2, Tube 3 and Tube 4 were labelled as A1 to A20, B1 to B20, C1 to C20 and D1 to D20, respectively.

3.2 Classification procedure

There were three stages involved in the classification process, which are pre-process of stress wave data set, classification and validation of formed clusters. The pre-processing stage includes filtering and feature selection based on the selected pre-process algorithm. The data were pre-processed to acquire the ideal description of the data patterns. Moreover, this helps to remove unnecessary data and reduces computational burden. In this paper, the AR coefficient was selected as the most appropriate feature to correspond to the stress wave signals for classification analysis. It was proposed that stress wave signals from the same tube condition (e.g., 20% defect depth, through-hole defect and others) could be clustered in well-defined groups. Then, stress wave signals were assigned according to certain clusters based on sequential stages of similarity and binary linkages.

The classification was made based on basic and incremental distance value of the pre-process feature. In the similarity stage, the Euclidean distance between every set of stress wave signal was measured and specified in the similarity matrix. It was followed by the binary linkage stage, where the information in the similarity matrix was used to create binary clusters. The formation of binary

cluster starts with the closest Euclidean distance between two stress wave signals until all stress wave signals were linked together in a hierarchical tree. Finally, validation was done to check whether the algorithm produced the optimal results. In this study, MATLAB was used as the signal processing software. The classification results were represented graphically using a dendrogram plot.

4. Results and discussion

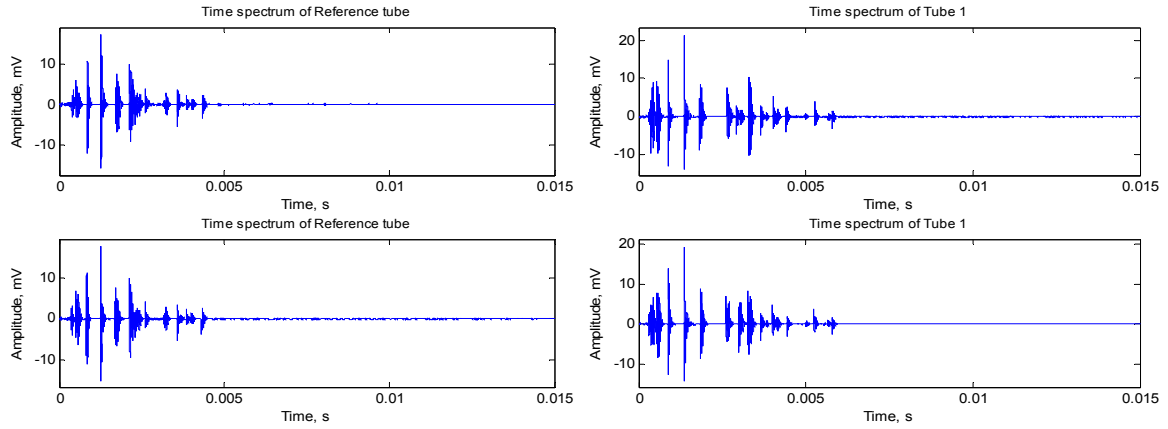
4.1 Stress wave time history

Each impact force load produced an individual stress wave signal. The stress waves associated with 20 impact force loads were collected. A typical defect-free stress wave signal acquired by the AE transducer when impact force load was applied to the reference tube is depicted in Fig. 7(a). In addition, the resultant stress wave signals captured from the defective tubes are demonstrated in Figs. 7(b)-(e). It is apparent from Figs. 7(a)-(e) that the stress wave attenuated as it propagated across the tube length. All the stress wave signals exhibited a periodical burst type, which started at a low amplitude until it reached the peak amplitude. It is followed by a more repetitive burst signal at a gradually lower amplitude until it completely attenuated. It is observed that the burst resembles the classic AE waveform produced by a Hsu-Nielson source (Baxter *et al.* 2007).

As shown in Figs. 7(a)-(e), the stress wave propagation in the defective tubes is more complicated than the stress wave propagation in the reference tube. Specifically, it is obvious that stress wave signals for the defective tubes contain more burst in the tail of the signals. Observations showed that the signal associated with the reference tube completely attenuated at $4,500 \mu\text{s}$. Therefore, the impact test with defective tubes was set to above $4,500 \mu\text{s}$ in order for the stress wave associated with defects to be monitored. Figs. 7(b)-(e) showed that the stress wave associated with the defect completely attenuated at a later time than the reference tube. The stress wave signals associated with Tube 1, Tube 2 and Tube 3 were completely attenuated at $6,000 \mu\text{s}$, $7,000 \mu\text{s}$ and $7,500 \mu\text{s}$ respectively, as demonstrated in Figs. 7(b)-(d). Tube 4 had the deepest defect depth attenuated at later time than $9,000 \mu\text{s}$ as shown in Fig. 7(e).

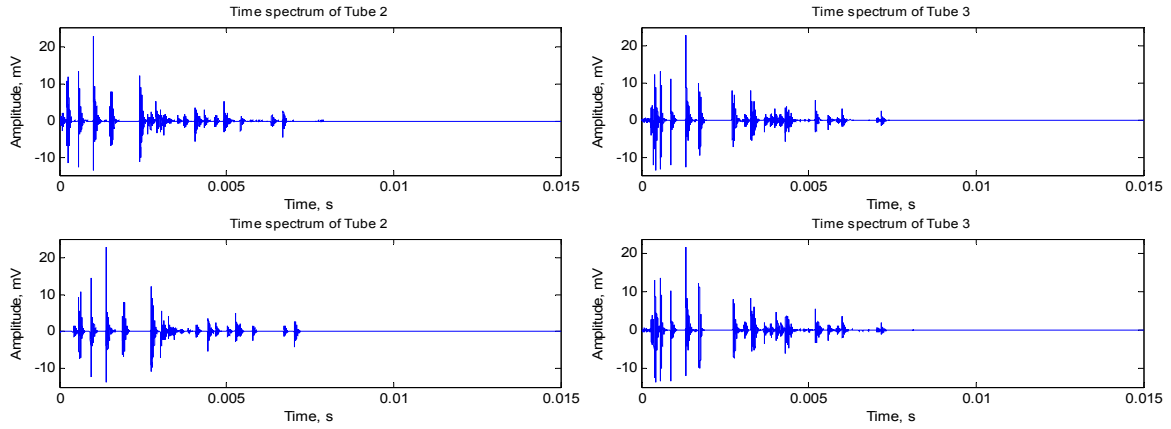
The stress wave signals for each of the tube condition exhibited a unique pattern. These findings support the idea of stress wave propagation in tube structures. The result suggested that the presence of defect disturbs the stress wave propagation path. As the depth of disturbance increases, more repetitive burst signals at lower amplitude can be observed in the stress wave signals. However, identifying the differences between stress wave signals for the defective tubes by visual inspection was more complicated. The differentiation was more complicated particularly as the peak amplitudes were very similar for all the tube conditions and the attenuation time do not vary very much from each other. The peak amplitude of a signal depends on many factors, such as the sensor coupling quality, the source energy, the signal attenuation, the sensor-source distance and the changes in wave propagation conditions.

Additionally, these results must be interpreted with caution. The possible difficulty when dealing with measured stress wave signals is to know the start and end of the signals. Therefore, adequate threshold setting is imperative for accurate measurement. Different threshold setting will lead to different arrival time and attenuation time. Setting a high threshold level could possibly result in the lost of important information on stress propagation. Any micro-changes with low peak amplitudes are unable to cross the high threshold. The signals will not be captured by the AE



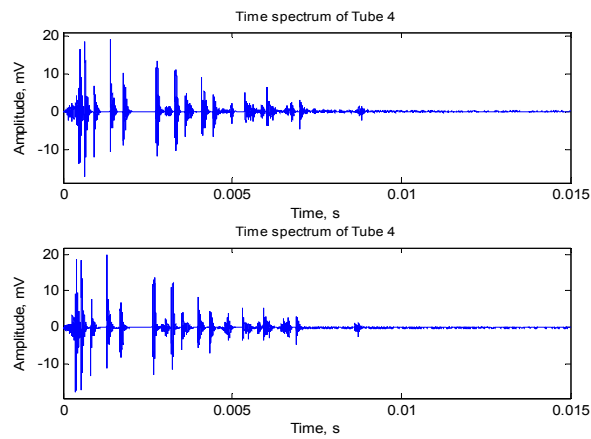
(a) Reference tube

(b) Tube 1



(c) Tube 2

(d) Tube 3



(e) Tube 4

Fig. 7 Stress wave time history

sensor. On the contrary, noise may intervene into the captured signals at lower threshold levels. Higher amplitude noise signals will be considered as part of the stress wave propagation. Hence, to overcome this issue, the optimum threshold is selected based on the background noise properties. An addition of 6 dB to the background noise level doubles the measured properties of the background noise.

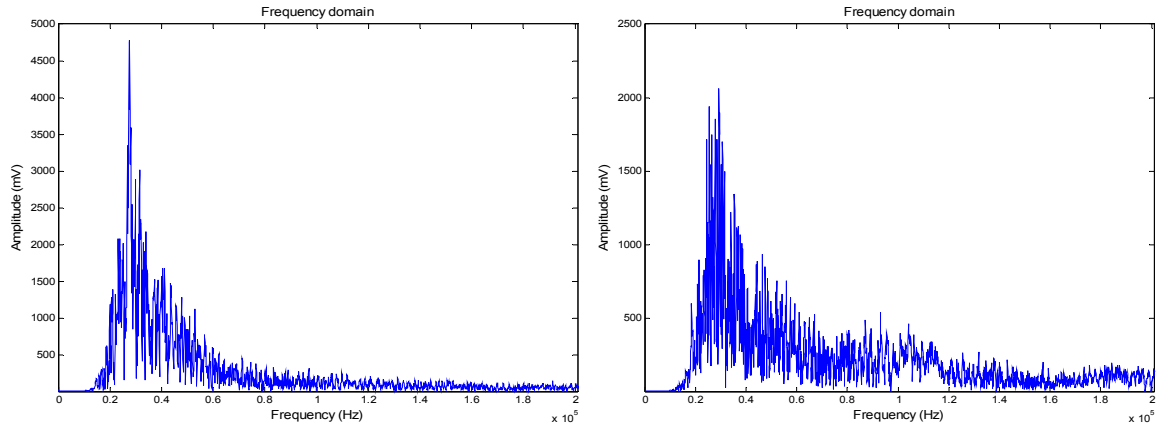
The frequency spectrum analysis has also been applied to all stress wave signals. The results of the corresponding frequency spectrum, for all tube conditions are shown in Fig. 8. Figs. 8(a)-(e) show that the frequency contents for all the tube conditions ranged from 18 kHz to 80kHz. This range is consistent with the frequency ranged derived from other impact tests using the impact hammer (Sansalone and Streett 1997). Moreover, the frequency content from the impact force load is in agreement with the measurement frequency range setting. Nonlinearity is not a crucial issue as the frequency content generated by the impact is within the measurement frequency setting.

Moreover, as the number of stress wave increases, a more efficient method was necessary to easily distinguish and compare the stress wave pattern. Previous research on the statistical parameters from resulted stress wave signals showed that r.m.s, kurtosis and crest factor could effectively distinguish tube condition (Zakiah *et al.* 2013). However, the variation in statistical parameter was very small. Thus, a more effective feature extraction technique to compliment the conventional statistical features is necessary. Pattern recognition based on stress wave signals is worthy to be considered to enable identification of tube condition.

4.2 Classification analysis

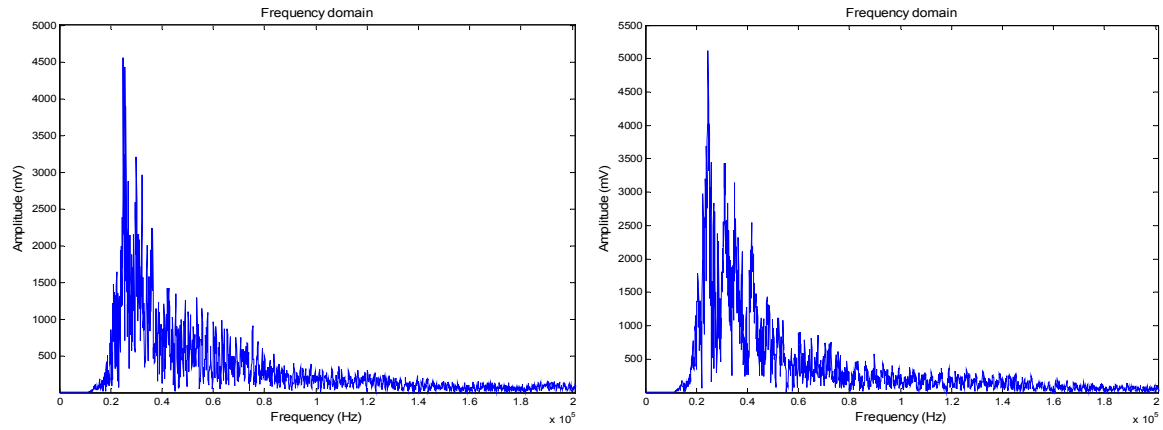
Classification of stress wave pattern based on the AR coefficient was performed in attempt to distinguish the stress wave signals of defective tubes from the stress wave signals of the reference tube. The AR algorithm was utilized to identify and classify the propagation of high stress wave signals in the tubes as these techniques were found to be capable of identifying hidden trends of complex stress waves and classifying a time-based signal based on the shape of the signal (Grad *et al.* 2004, Jamaludin and Mba 2002a, b). These researches showed that AR coefficients have appropriate attributes to characterise the shape of a stress wave signal. Besides, AR coefficients are independent of signal amplitude. It is noticeable from the resultant stress wave that a tube of different defect depth has a different stress wave propagation path; hence, the signal captured is different from one another. The classification analysis is interesting in determining the major types of stress wave signals and their characteristics. In addition, this study was attempted to assess whether the AR coefficient was adequate to group the stress wave signals into the right cluster groups to correspond to different depths of defects, since it is known that stress wave propagation is affected by the presence of disturbance.

The AR clustering algorithm was tested to find reasonable clusters without looking at all relationships. The AR coefficient becomes the signal feature that estimates the shape of stress wave signals. Hence, it is essential to determine the model order of AR coefficients that sufficiently represent each stress wave signal. FPE was performed on the stress wave signals to determine the correct model order. It is essential that all stress wave signals associated with each tube condition have the same model order input to characterise the shape of the stress wave signal. The shape of a stress wave signal can be characterised by the AR coefficients as long as the model order is sufficiently large. As shown in Fig. 9(a), FPE performed on stress wave signals of the reference tube showed that a model order of 40 was sufficient to characterise the shape of stress wave signal. As displayed in Figs. 9(b)-(e), the same results were obtained when FPE was applied



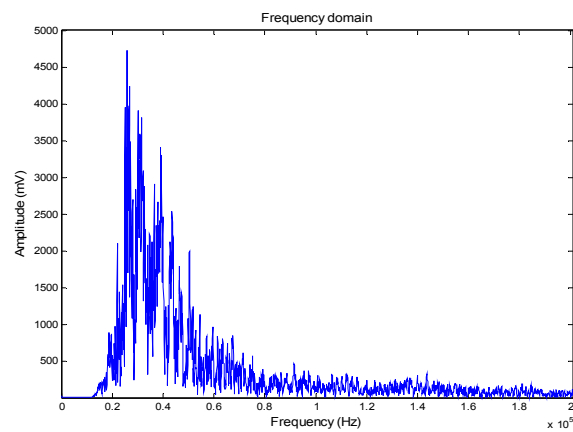
(a) Reference tube

(b) Tube 1



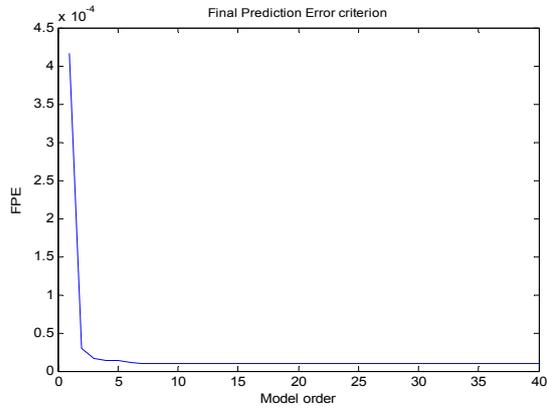
(c) Tube 2

(d) Tube 3

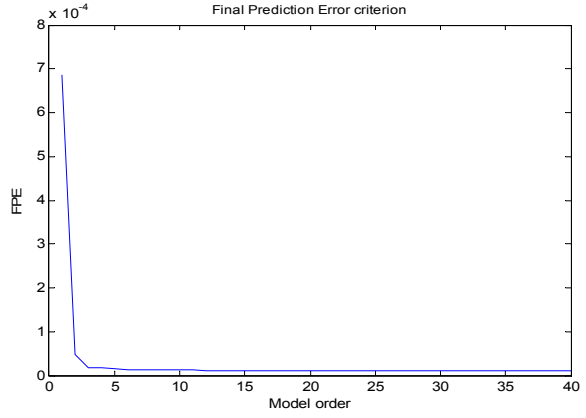


(e) Tube 4

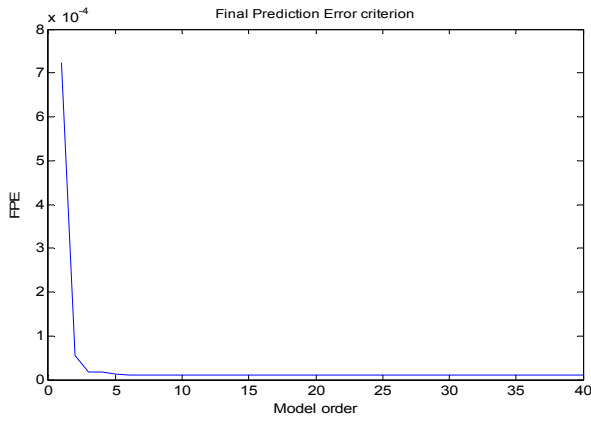
Fig. 8 Frequency spectrum for test tubes



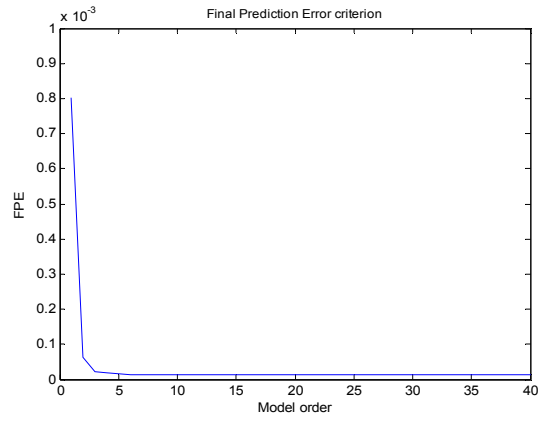
(a) Reference tube



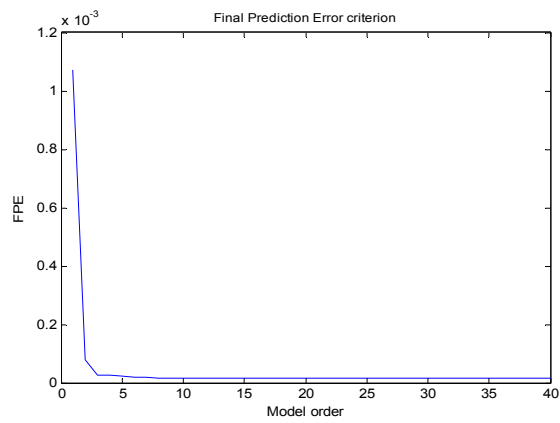
(b) Tube 1



(c) Tube 2



(d) Tube 3



(e) Tube 4

Fig. 9 Final prediction error

to stress wave signals associated with defective tubes. The use of high model order usually has insignificant effect on the spectral evaluation. However, underestimating the model order can alter the evaluation significantly. Hence, overestimating the model order is better than underestimating it (Thanagasundram and Schlindwein 2006b). Therefore, it is proposed that a model order of 40 was adequate to predict the shape of stress wave signals.

The classification process utilised the K-means clustering technique. The K-means clustering involves the process of separating items into its natural groups with the intention that each items has similar characteristics and are distinct from different groups (Žalik 2008, Godin *et al.* 2004). The clustering was achieved by measuring the Euclidean distances between each stress wave signal and using Ward's method to group the AR coefficients associated with each stress wave signal. Euclidean distance was chosen to represent the similarity measure between each stress wave signal. In this paper, Ward's method of clustering was utilized rather than the centroid linkage. Ward's method was selected as it produces approximately the same number of observations in a cluster. This method is appropriate to reflect an equally-sized cluster. Moreover, it is effective in improving the homogeneity within each group and avoids chaining or non-monotonic clustering.

Each stress wave signal was linked to a set of AR coefficients determined by FPE. In this study, 40th AR model order implies that every stress wave signal was associated with 41 AR coefficients. Initially, the error sum of squares (ESS) of every AR coefficient in the cluster was computed. Then, the ESS of individual AR coefficients was compared against the cluster's centroid. The pair of AR coefficients that produced the smallest ESS will create the first cluster. A small ESS implies that the AR coefficients were close to their cluster centroid, suggesting that the AR coefficients have similar profiles. Then, a new set of AR coefficients was added to the cluster and the new ESS was computed. AR coefficients with minimum ESS were gathered into the newly created cluster. The ESS of the cluster was changed whenever a new set of AR coefficients were added to the existing cluster. This step was repeated until all the stress wave signals were clustered together, starting with the adjacent two stress wave signals. The selection of which two clusters to combine was based on which combination of clusters minimized in the ESS across all stress wave signals in all cluster.

The dendrogram plot was used to graphically present the classification results in this study. The dendrogram is a two-dimensional diagram that portrays the results of classification. The x-axis in the dendrogram plot represents the values of ESS at which the mergers occur and the y-axis shows the individual labelled stress wave signals. Stress wave signals for the reference tube were labelled as R1 to R20, while stress wave signals produced in the defective tubes were labelled as signals A1 to A20 for Tube 1, B1 to B20 for Tube 2, C1 to C20 for Tube 3, D1 to D20 for Tube 4. The classification results are depicted using the dendrogram plots in Figs. 10(a)-(d).

The use of AR coefficients as the input stress wave signal produced successful recognition between stress wave signals from the reference tube and defective tubes. The classification results as depicted in Fig. 10(a)-(d) showed that the resulted stress wave signals propagating along the tube structures were clustered into two main groups. Fig. 10(a) shows the dendrogram plot for the classification result of the stress wave signals associated with the reference tube and Tube 1. It was apparent that two main groups differentiate between the stress wave signals for the reference tube and Tube 1. The cluster has been labelled for easy reference. Stress wave signals from the reference tube were clustered together in Cluster R while stress wave signals from Tube 1 were assembled together in Cluster A. The groups labelled R1 to R20 represented all 20 stress wave signals of similar propagation paths from the reference tube as identified by the classification

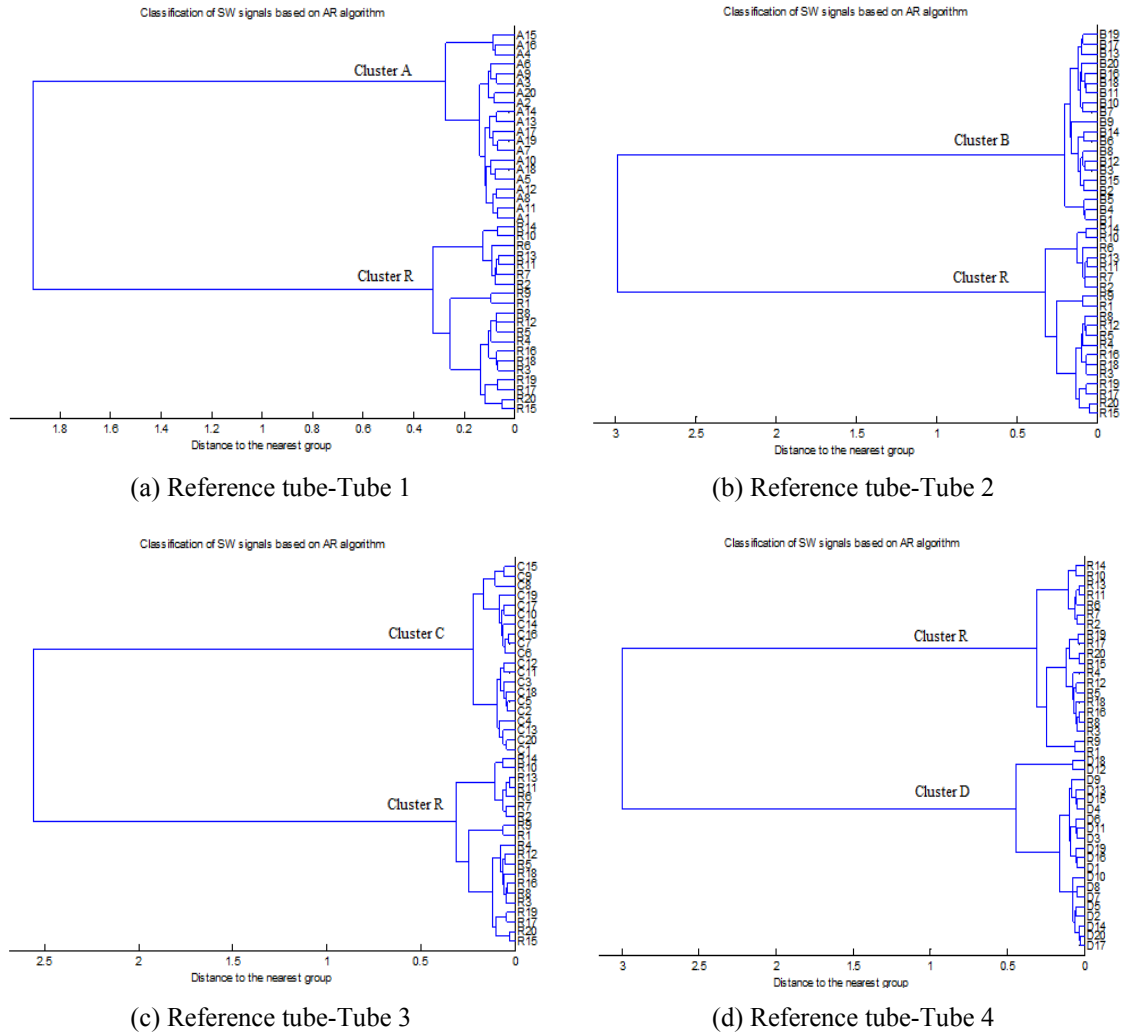


Fig. 10 Classification analysis using AR algorithm

analysis. A close examination suggested that these 20 stress wave signals have similar stress wave history and attenuation time in the sense that stress wave signals produced by similar impact forces tend to have similar characteristics and propagation paths.

The classification result for the stress wave signals associated with the reference tube and Tube 2 is displayed in Fig. 10(b). The resulted dendrogram demonstrated that stress wave signals were effectively gathered into two primary groups associated with tube condition. Stress wave signals for the reference tube were effectively grouped together in Cluster R, whereas stress wave signals for Tube 2 were grouped into Cluster B. A similar result was observed for stress wave signals associated with the reference tube and the other defective tubes, Tube 3 and Tube 4 as indicated in Figs. 10(c)-(d), respectively. Stress wave signals associated with the reference tube were merged together in Cluster R while stress wave signals associated with the defective tubes were assembled together in Cluster C and Cluster D.

A further examination of the maximum group distance criterion (MGDC) suggested by Jamaludin (2000) reveals an interesting result. The MGDC measures the maximum Euclidean distance between the main groups from the resulted dendrograms. The value quantifies how the main groups vary from each other in the representative dendrograms. The MGDC for all the tube conditions are tabulated in Table 2. As can be seen in Table 2, an increase in the depth of defect resulted in an increase in the MGDC values. The healthy tube and Tube 1 have the lowest MGDC value. Meanwhile, reference tube-Tube 2 and reference tube-Tube 4 have the highest MGDC value of 3. Surprisingly, Tube 3 with 60% defect depth was found to have less MGDC compared to Tube 2 that has a narrower defect depth (40%) when both were evaluated contrasted over with the healthy tube.

In the next section, classification between all stress wave signals of the tubes was also carried out to investigate whether the AR classification analysis could be utilised to identify the presence of defect in the tubes. The result depicted in Fig. 11 shows that stress wave signals are effectively classified into two well-defined clusters that differentiate the stress wave signals of the reference tube and the defective tubes. The classification result showed that all stress wave signals from the

Table 2 Maximum group distance criterion

Tube	MGDC
Reference tube & Tube 1	1.9
Reference tube & Tube 2	3.0
Reference tube & Tube 3	2.5
Reference tube & Tube 4	3.0

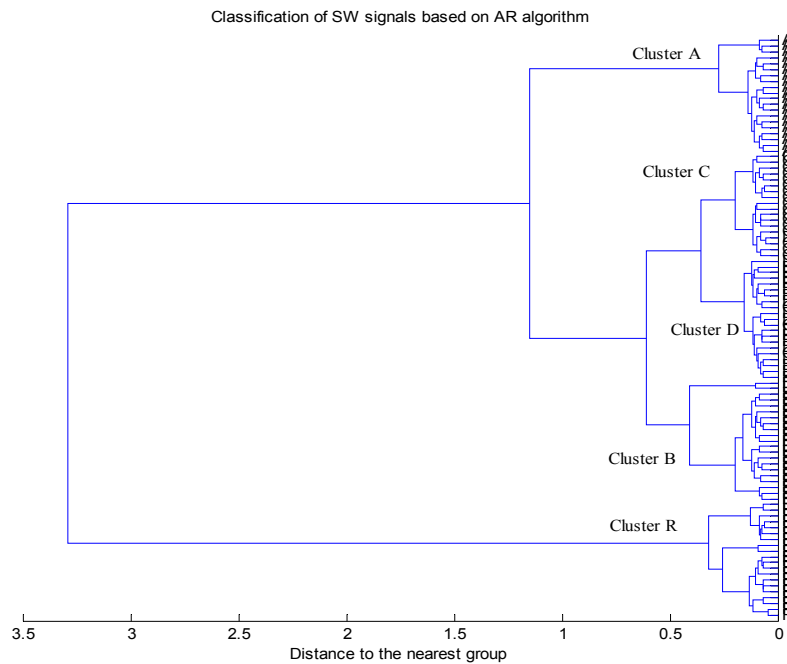


Fig. 11 Classification of all stress wave signals

reference tube were properly classified in Cluster R. On the other hand, stress wave signals from the defective tubes of Tube 1, Tube 2, Tube 3 and Tube 4 tend to merge together into another major cluster.

Each group of stress wave signals from the defective tubes were identified in small cluster groups A, B, C and D. Cluster A effectively clustered together all stress wave signals associated with Tube 1. In Cluster B, 90.5% of the stress wave signals were associated with Tube 2 and 9.5% were stress wave signals associated with Tube 4. It could be concluded that Cluster B was dominated by the stress wave signals associated with Tube 2. Cluster C consists of 18 stress wave signals. It was dominated by 94.4% stress wave signals associated with Tube 3 and 5.6% stress wave signals associated with Tube 4. Cluster D consists of 81% stress wave signals associated with Tube 4, 14.3% stress wave signals associated with Tube 3 and 4.7% stress wave signals associated with Tube B. Hence, it was suggested that Cluster A, Cluster B, Cluster C and Cluster D represent stress wave signals associated with Tube 1, Tube 2, Tube 3 and Tube 4, respectively.

Several stress wave signals from Tube 3 and Tube 4 were observed to be clustered in different clusters. This phenomenon was attributed to the inconsistent strength of the applied impact force in the associated tube condition. Therefore, stress wave signals with different patterns were generated as the results of variation in the impact forces. Stress wave signals were severely impaired when the measured stress wave signals were changed due to inconsistency in impact force load. Apart from being attributed by the variation of the strength of impact forces, this phenomenon was probably due to the depth between the defects. It is expected that the classification results will become more apparent when the impact load was consistently applied and larger tube wall thickness was used. This will attribute to more apparent and distinctive stress wave signals between the defective tubes. A comparison of the MGDC of each cluster with the healthy tube is presented in Table 3. These results signified that a higher MGDC value reveals a greater deviation from the reference tube. Besides, the MGDC between the defective tubes had smaller variation. These findings help us to understand the pattern of stress wave propagation in tube structure when disturbance is present in the tube. However, more research in this topic needs to be undertaken before the association between MGDC and depth of defect is understood.

It is clear that these results have achieved the aim of classification. Primarily, the presence of two large groups has discriminated the stress wave signals of the reference tube and the defective tubes. This is justified from the stress wave signals that the defective tubes have different transmission path compared to the reference tube. Secondly, AR method has proven to be sufficiently sensitive to split stress wave signals into the right cluster group. This signifies that the AR algorithm can distinguish stress wave signals between the defective tubes and the reference tube.

The success of AR coefficients to differentiate the stress wave signals from defective tubes from the reference tube signals was primarily due to the distinctive stress wave signal patterns in

Table 3 Maximum group distance criterion for combination of all tube conditions

Tube	MGDC
Reference tube & defective tubes (Cluster a, Cluster B, Cluster C and Cluster D)	3.3
Cluster A & Cluster B, Cluster C and Cluster D	1.2
Cluster B & Cluster C and Cluster D	0.6
Cluster C & Cluster D	0.3

the inspected tubes. The distinctive stress wave signals pattern of the defective tubes was attributed to the energy loss mechanism of stress wave in the tube structure, which can be the combination of reflection, diffraction and/or dispersion from the defect presence in the structure (Sansalone 1997, Schubert *et al.* 2004). Moreover, as the depth of defect increases, more stress wave is reflected and diffracted in numerous direction and extends the attenuation of stress wave signals in the defective tubes. Defective tubes have longer propagation path. Tubes with through-hole defect have the longest propagation paths. Hence, the AR algorithm could be utilised as an identification tool to determine the presence of defect in the tubes by identifying which group the measured signals are clustered. Moreover, the classification of results using AR coefficients is consistent with the statistical features analysis that noticeably separated the defective tubes from the reference tube (Zakiah *et al.* 2013).

AR clustering also made the inferential much easier. The relationships shown in the dendrogram can be used to characterise the stress wave signal patterns of the impacted tubes and identify stress wave signals of defective and reference tubes. The classification analysis results have shown that stress wave signals propagating along the tube structures could be effectively classified into two distinct groups using AR coefficient. The classification results validated that the defective tubes have different propagation stress wave path in contrast to the reference tube. AR coefficients have the capability of recognising and differentiating the transmission path provided by different depths of defects.

The classification results using AR coefficients are solely based on visual inspection using dendrograms as proposed by (Jamaludin and Mba 2002a, b) and (Hall and Mba 2004). The judgment to differentiate between the reference tube and defective tubes condition was accomplished based on the visual interpretation of the dendrograms. The classification results for all stress wave signals from different tube conditions revealed that the stress wave signatures associated with the reference tube were well-separated from the defective tube condition. The finding of this research showed a quick evaluation of defect can be achieved from the illustrative dendrograms. The dendrogram allows easy assessment of the nature of stress wave signals. The dendrograms are valuable to aid in understanding the stress wave signals and prevent false interpretation problems. The dendrogram can quickly and confidently interpret and identify the presence of defect. The dendrogram illustrates the mergers or divisions of stress wave signals that have been made at succeeding clustering levels, as well as the pictorial view of cluster formation. This approach easily discovers the difference between complex stress wave signals and translates it into quick decisions based on visual inspection. The dendrogram becomes an alternative presentation to portray the groups of stress wave signals compared to the current practice of comparing the defective signals with the reference signals.

The classification results demonstrated the versatility of AR algorithm. The results may therefore appear optimistic for different type of defect such as U-shaped notches, crack and corrosion. We believe that the AR algorithm should be reliable to correctly classify the stress wave captured from different types of defects. The presence of other types of defects will affect the stress propagation paths, and consequently the shape of the signals. The AR algorithm in this study provides a foundation for future studies for on different types of tube defects.

Additionally, in this study, several variables such as support condition, length of tubes, fixed impact load, as well as similar tube properties were fixed. Different support condition and impact load may affect the stress wave propagation in the tubes. Moreover, the length of the tubes and material properties of the tubes may significantly impinge on the stress wave propagation. Besides, the stress wave data obtained from the VIAE technique were under controlled laboratory condition.

The background noise in industrial site may severely influence the threshold level setting. The application of the AR algorithm to the stress wave obtained from the real application is imperative to access the validity of the proposed technique. There is abundant room for further progress in determining the applicability of the AR algorithm in real application. Further studies, which take these variables into account, will need to be undertaken.

5. Conclusions

A classification analysis of stress wave signals based on the AR algorithm has been proposed in this study.

- The resultant stress wave signals associated with different depths of defects were unique and distinct from each other.
- The application of AR classification in discriminating the measured stress wave signals of the defective tubes from the reference tube has been verified.
- The proposed AR algorithm technique effectively classified the unique characteristic feature associated with stress wave signals.
- The application of AR coefficients to stress wave signals enables recognition of suitable clusters, which reflects the identity of the cluster.
- Classification of defect using AR coefficients has shown to provide quick and easy defect identification, and automate interpretation results of VIAE technique.
- The resulted dendrogram demonstrated the ability of the AR algorithm to automate tube defect detection is possible and promising. However, more work is required before application in industry.
- This study can be considered as the first investigative step since it concerns a single application of the method to specific type of tubes and to unique specimens and therefore its effectiveness has to be proven with further investigations.
- This method could be extended to different types of tubes, material properties, supporting condition and environment as long as the tube surface is accessible to attach the sensor and apply impact load.
- This method could also be applicable for discriminating different types of defects.
- The selection of sensor location in real industry is critical. The sensor should be located at the end of the tube length to capture the stress wave propagation along the tube structure.

Acknowledgments

The research materials described in this paper was supported by the Tenaga Tiub Sdn. Bhd. The student is financially supported by Universiti Teknikal Malaysia Melaka and Jabatan Pengajian Tinggi, Kementerian Pendidikan Malaysia.

References

- Allahkaram, S.R., Zakersafae, P. and Haghgoo, S.A.M. (2011), "Failure analysis of heat exchanger tubes of four gas coolers", *Eng. Fail. Anal.*, **18**(3), 1108-1114.

- Antaki, G.A. (2005), *Piping and Pipeline Engineering-Design, Construction, Maintenance, Integrity, and Repair*, Marcel Dekker, Inc., New York, NY, USA.
- Atamturktur, S., Bornn, L. and Hemez, F. (2011), "Vibration characteristics of vaulted masonry monuments undergoing differential support settlement", *Eng. Struct.*, **33**(9), 2472-2484.
- Baxter, M.G., Pullin, R., Holford, K.M. and Evans, S.L. (2007), "Delta T source location for acoustic emission", *Mech. Syst. Signal Process.*, **21**(3), 1512-1520.
- Birchall, M. (2007), "Internal ultrasonic pipe & tube inspection – IRIS", *IV Conferencia Panamericana de END*, Buenos Aires, Argentina, October.
- Birring, A.S. (1999), "Selection of NDT techniques for inspection of heat exchanger tubing", *ASNT International Conference on Petroleum Industry Inspection*, Houston, TX, USA, June.
- Broersen, P.M.T. (2006), *Automatic Autocorrelation and Spectral Analysis*, Springer-Verlag, London, United Kingdom.
- Bulloch, J.H., Callagy, A.G., Scully, S. and Greene, A. (2009), "A failure analysis and remnant life assessment of boiler evaporator tubes in two 250MW boilers", *Eng. Fail. Anal.*, **16**(3), 775-793.
- Carino, N.J. (2013), "Training: Often the missing link in using NDT methods", *Construct. Build. Mater.*, **38**, 1316-1329.
- Chen, X., He, Z. and Xiang, J. (2005), "Experiments on crack identification in cantilever beams", *Experim. Mech.*, **45**(3), 295-300.
- Cicero, S., Lacalle, R., Cicero, R. and García, J. (2010), "Failure analysis of a steam generator superheater drain tube used in a dump", *Eng. Fail. Anal.*, **17**(1), 301-312.
- Da Silva, J.J., Lima, A.M.N., Neff, F.H. and Neto, J.S. (2009), "Non-invasive fast detection of internal fouling layers in tubes and ducts by acoustic vibration analysis", *IEEE Trans. Instrument. Measure.*, **58**(1), 108-114.
- Da Silva, R.R., Soares, S.D., Calôba, L.P., Siqueira, M.H.S. and Rebello, J.M.A. (2006), "Detection of the propagation of defects in pressurised pipes by means of the acoustic emission technique using artificial neural networks", *Insight-Non-Destructive Test. Condition Monit.*, **48**(1), 45-51.
- Elforjani, M. and Mba, D. (2010), "Accelerated natural fault diagnosis in slow speed bearings with acoustic emission", *Eng. Fract. Mech.*, **77**(1), 112-127.
- Gao, Y., Brennan, M.J., Joseph, P.F., Muggleton, J.M. and Hunaidi, O. (2005), "On the selection of acoustic/vibration sensors for leak detection in plastic water pipes", *J. Sound Vib.*, **283**(3-5), 927-941.
- Godin, N., Huguet, S., Gaertner, R. and Salmon, L. (2004), "Clustering of acoustic emission signals collected during tensile tests on unidirectional glass/polyester composite using supervised and unsupervised classifiers", *NDT & E International*, **37** (4), 253-264.
- Gotoh, Y. and Takahashi, N. (2007), "Three-dimensional FEM analysis of electromagnetic inspection of outer side defects on steel tube using inner coil", *IEEE Trans. Magn.*, **43**(4), 1733-1736.
- Grad, L., Grum, J., Polajnar, I. and Slabe, J.M. (2004), "Feasibility study of acoustic signals for on-line monitoring in short circuit gas metal arc welding", *Int. J. Mach. Tool. Manuf.*, **44** (5), 555-561.
- Hall, L.D. and Mba, D. (2004), "Acoustic emissions diagnosis of rotor-stator rubs using the KS statistic", *Mech. Syst. Signal Process.*, **18** (4), 849-868.
- Haritos, N. and Owen, J.S. (2004), "The use of vibration data for damage detection in bridges: a comparison of system identification and pattern recognition approaches", *Struct. Health Monitor.*, **3**(2), 141-163.
- Jamaludin, N. (2000), "Monitoring low speed rolling element bearing using stress waves technique", Ph.D. Dissertation; Cranfield University, Bedford, UK.
- Jamaludin, N. and Mba, D. (2002a), "Monitoring extremely slow rolling element bearings: Part I", *NDT & E International*, **35**(6), 349-358.
- Jamaludin, N. and Mba, D. (2002b), "Monitoring extremely slow rolling element bearings: Part II", *NDT & E International*, **35**(6), 359-366.
- Lee, T.H., Choi, I.H. and Jhang, K.Y. (2008), "Single-mode guided wave technique using ring-arrayed laser beam for thin-tube inspection", *NDT & E International*, **41**(8), 632-637.
- Mahjoob, M.J., Shahsavari, A. and Marzban, A. (2007), "A vibration-based damage detection method for pipes conveying fluid", *Proceedings of the 48th AIAA/ASME/ASCE/AHS/ASC Structures, Structural*

- Dynamics, and Materials Conference*, Hawaii, USA, April.
- Ryu, K., Son, D., Park, D. and Jung, J. (2009), "Reactance change at defect in Inconel tube with nickel sleeving", *IEEE Trans. Magn.*, **45**(6), 2733-2735.
- Sansalone, M. (1997), "Impact-echo: The complete story", *ACI Struct. J.*, **94**(6), 777-786.
- Sansalone, M. and Streett, W.B. (1997), *Impact-echo: Nondestructive Evaluation of Concrete and Masonry*, Bullbrier Press, Ithaca, NY, USA.
- Schubert, F., Wigggenhauser, H. and Lausch, R. (2004), "On the accuracy of thickness measurements in impact-echo testing of finite concrete specimens-numerical and experimental results", *Ultrasonics*, **42**(1-9), 897-901.
- Shehadeh, M.F., Abdou, W., Steel, J.A. and Reuben, R.L. (2008), "Aspects of acoustic emission attenuation in steel pipes subject to different internal and external environments", *Proceedings of the Institution of Mechanical Engineers, Part E: J. Process Mech. Eng.*, **222**(1), 41-54.
- Thanagasundram, S. and Schlindwein, F.S. (2006a), "Autoregressive based diagnostics scheme for detection of bearing faults", *Proceedings of ISMA*, Belgium, September.
- Thanagasundram, S. and Schlindwein, F.S. (2006b), "Autoregressive order selection for rotating machinery", *Int. J. Acoust. Vib.*, **11**(3), 1-11.
- Wilson, J.W. and Tian, G.Y. (2007), "Pulsed electromagnetic methods for defect detection and characterisation", *NDT & E International*, **40**(4), 275-283.
- Xueqin, L., Gang, L. and Shangqing, L. (2008), "The development of the boiler water wall tube inspection", *Third International Conference on Electric Utility Deregulation and Restructuring and Power Technologies DRPT 2008*, Nanjing, China, April.
- Yang, B. and Li, X. (2013), "Pulsed remote field technique used for nondestructive inspection of ferromagnetic tube", *NDT & E International*, **25**(1), 3-12.
- Zakiah, A.H., Jamaludin, N., Syarif, J. and Yahya, S.Y.S. (2013), "Detection and analysis of defect in steel tube using Vibration Impact Acoustic Emission (VIAE) method", *Int. Rev. Mech. Eng.*, **8**(1), 277-282.
- Žalik, K.R. (2008), "An efficient k' -means clustering algorithm", *Pattern Recogn. Lett.*, **29**(9), 1385-1391.
- Zhan, Y.M. and Mechefske, C.K. (2007), "Robust detection of gearbox deterioration using compromised autoregressive modeling and Kolmogorov–Smirnov test statistic—Part I: Compromised autoregressive modeling with the aid of hypothesis tests and simulation analysis", *Mech. Syst. Signal Process.*, **21**(5), 1953-1982.
- Zhang, Y., Ye, Z. and Xu, X. (2007), "An adaptive method for channel equalization in MFL inspection", *NDT & E International*, **40**(2), 127-139.